Clays and Clay Minerals, Vol. 45, No. 3, 428–439, 1997.

CHARACTERIZATION OF IRON-MANGANESE CONCRETIONS IN KENTUCKY ALFISOLS WITH PERCHED WATER TABLES

MIN ZHANG AND A. D. KARATHANASIS

Department of Agronomy, N-122K Agr. Science-North, University of Kentucky, Lexington, Kentucky 40546-0091

Abstract—Iron-manganese concretions are common in upper sola of Alfisols in the Inner Bluegrass Region of Kentucky. Their nature and quantities appear to be related to the fluctuation of seasonal perched water tables above clayey argillic horizons. This study was conducted to examine changes in the macro-and micromorphology, chemistry and mineralogy of concretions as a function of size, color and soil depth. Total Mn and Fe contents increased, while SiO_2 decreased with concretion size. Black concretions contained higher Mn, while brown concretions were higher in Fe. Crystalline Mn- and Fe-oxides fractionated with a sequential extraction procedure increased, but amorphous Mn and Fe decreased with concretion size. Goethite was the only crystalline Fe oxide mineral identified by X-ray diffraction (XRD) analysis. Manganese oxide minerals were very difficult to detect due to the diffuse nature of their XRD peaks and poor crystallinity. Examination of soil thin sections showed concretions of soil horizons overlying restrictive clayey layers to exhibit differentiated fabrics, sharp external boundaries and generally spherical shapes. Concretions found within clayey restrictive layers or above lithic interfaces usually had less structural organization, softer matrices and diffuse external boundaries due to longer term saturated conditions. Scanning electron microscopy (SEM) examinations suggested that the concretionary matrix, in spite of its density, has numerous cavities and an extensive micropore system within which dissolved plasmic Fe and Mn can diffuse and precipitate.

Key Words—Elemental Composition, Fractionation, Micromorphology, Mineralogy.

INTRODUCTION

Iron and Mn concretions have been found in many soils, and especially in soils with restrictive internal drainage. The quantity, chemical composition, mineralogy and size of concretions in soils are site-specific depending on the action of weathering processes for that location (Drosdoff and Nikiforoff 1940; Gallaher et al. 1973a, 1973b; Rhoton et al. 1991; McDaniel et al. 1992). Many researchers define concretions as mixtures of soil materials cemented together (Winters 1938; Radden and Porter 1962; Murthy and Mathur 1964). The cementing agents for Fe-Mn concretions are Fe and Mn oxides. Therefore, the concretionary material is characterized by a greater concentration of Fe and Mn oxides than the surrounding soil matrix (Barnhisel et al. 1969; Phillippe et al. 1972; Rhoton et al. 1993). It also differs from the surrounding soil matrix by containing less SiO_2. Schwertmann and Fanning (1976) found that Mn and Fe are not evenly distributed in all concretions found within a given soil horizon or even within a given concretion. Manganese content is usually related to concretion size, with larger concretions containing more Mn and lower Fe/Mn ratios. Also, dark-colored concretions are generally higher in Mn content than lighter-colored concretions (Phillippe et al. 1972), but color, shape and hardness may differ among different soils. Concretions found in the better-drained soils of loess hydrosequences in Bavaria were usually rusty-colored with a blackish interior, irregular in shape and medium in hardness. However, in soils with restrictive layers, black, well-rounded and hard concretions prevailed in the upper part of the profile, whereas in deeper horizons the concretions were similar to those in the drier soils (Schwertmann and Fanning 1976).

The effect of concretion accumulation on soil chemical properties could be significant at high concentrations, depending on the chemistry and mineralogy of the oxide components. In several studies, goethite was the only Fe-oxide mineral identified by XRD in concretionary materials (Gallaher et al. 1973b; Schwertmann and Fanning 1976; Rhoton et al. 1993). Manganese oxides were found to be fine-grained with relatively diffuse XRD peaks due to their poor crystallinity and low concentration (Tokashiki et al. 1986). Morphologically, most Mn oxides have a platy structure (birnessite and lithiophorite) or lathlike morphology (todorokite) and, if adequately crystalline, should respond to parallel orientation of XRD specimens (Ross et al. 1976). Uzochukwu and Dixon (1986) identified 2 Mn oxide minerals, birnessite and lithiophorite, by XRD in nodules of a Vertic Argiustoll in Texas using a magnetic concentration technique. Two Fe-oxide minerals, goethite and hematite, were also present in the nodular material.

Microscopic studies have shown that concretions of somewhat poorly drained soils are characterized by undifferentiated fabric and diffuse external boundaries. In contrast, concretions of well-drained soils are usually spherical with sharp external boundaries and differentiated fabric (Phillippe et al. 1972). Scanning

Table 1. Characteristics of the sites sampled.

Site	Pedon	Landscape position	Depth to bedrock (cm)	Slope gradient	Classification
POFA	POFA1	Upper sideslope	125	8%	Hagerstown, fine, mixed, mesic Typic Hapludalfs
	POFA2	Lower sideslope	90	7%	Faywood, fine, mixed, mesic Typic Hapludalfs
POFB	POFB1	Upper sideslope	122	9%	Hagerstown, fine, mixed, mesic Typic Hapludalfs
	POFB2	Lower sideslope	155	7%	Hagerstown, fine, mixed, mesic Typic Hapludalfs
STF	STF1	Upper sideslope	152	6%	Caleast, fine, mixed, mesic Mollic Hapludalfs
	STF2	Lower sideslope	115	6%	Caleast, fine, mixed, mesic Mollic Hapludalfs
SRF	SRF	Upper sideslope	>350	10%	Maury, fine, mixed, mesic Typic Paleudalfs

electron microscopic examinations of concretions showed them to be dominated by small irregularly shaped pores. The concretion fabric components, for the most part, were masked by massive plasmic depositions, indicating that much of the original matrix porosity had probably been infilled during the concretion formation process (Cescas et al. 1970).

The objectives of this study were: 1) to determine changes in physical, chemical and mineralogical composition of concretions with different size and color found in different horizons of perched water table-affected soils; and 2) to examine micromorphological features and structures related to their compositional characteristics.

MATERIALS AND METHODS

Profile samples were collected from 4 sites, including 7 pedons representing 4 soil series in the Inner Bluegrass Region of Kentucky. Characteristics of the sites sampled are given in Table 1 and Figure 1. The sampled pedons included 4 upper sideslope positions and 3 lower sideslope positions. The soils were classified as Hagerstown (fine, mixed, mesic Typic Hapludalfs), Faywood (fine, mixed, mesic Typic Hapludalfs), Caleast (fine, mixed, mesic Mollic Hapludalfs) and Maury (fine, mixed, mesic Typic Paleudalfs). Iron-Mn concretions were separated from air-dried soil samples by wet shaking overnight and wet sieving on a set of sieves with openings of 2, 1, 0.5 and 0.25 mm, respectively. Deionized water sprayed onto the concretions readily removed the soil particles. The concretions were separated into coarse (>2 mm), medium (2 to 1 mm), fine (1 to 0.5 mm) and very fine (0.5 to 0.25 mm) sizes. Coarse and medium concretions were separated from other fragments by visual inspection following hand-picking with tweezers, while fine and very fine concretions were separated using a strong magnet. Some coarse and medium concretion fractions were also separated into black and brown color groups by hand-picking with tweezers.

Concretions used for Mn and Fe fractionation were ground with an agate mortar and pestle until the entire sample passed through a 0.5-mm sieve. The fractionation of Mn and Fe was accomplished using a sequential extraction procedure proposed by Shuman (1985) and modified by McDaniel and Buol (1991). The secondary Mn and Fe were separated into exchangeable (EXCH), organic (OM), crystalline Mn oxide (MnCRO), Fe coprecipitated with Mn

Table 2. Mean values of elemental composition and analysis of variance for different size and color Fe-Mn concretions from selected horizons of the studied pedons.

Elemental oxide	Concretion size			Concretion color			Analysis of variance		
	Coarse (>2 mm) (n = 11)	Medium (2–1 mm) (n = 11)	Fine (1–0.5 mm (n = 11)	Black (n = 6)	Brown (n = 6)	Mixed (n = 21)	Size	Color	CV (%)
SiO_2	41.11[a]‡	46.89[b]	51.86[c]	46.58[a]	42.33[b]	47.88[a]	**†	**	6.8
Al_2O_3	14.44[a]	15.01[a]	14.58[a]	17.30[a]	14.82[b]	13.89[b]	NS	**	11.8
Fe_2O_3	33.76[a]	30.29[a]	26.43[b]	23.58[b]	36.05[a]	30.31[a]	*	**	18.7
MnO	7.19[a]	4.83[a]	3.84[a]	9.74[a]	2.24[b]	3.93[b]	NS	*	101.3
CaO	1.35[a]	1.15[a]	2.22[a]	1.50[a]	2.92[ab]	1.21[b]	NS	**	91.4
MgO	0.47[a]	0.45[a]	0.45[a]	0.48[ab]	0.54[a]	0.43[b]	NS	*	19.1
K_2O	0.95[a]	0.92[a]	0.88[a]	1.07[a]	1.04[a]	0.84[b]	NS	**	14.1
Na_2O	0.32[a]	0.27[a]	0.35[a]	0.54[a]	0.38[ab]	0.23[b]	NS	*	69.7
TiO_2	0.95[a]	0.88[a]	0.88[a]	0.80[b]	0.84[ab]	0.95[a]	NS	*	14.6
P_2O_5	0.61[a]	0.55[a]	0.60[a]	0.55[b]	0.77[a]	0.55[b]	NS	*	28.9
Fe_2O_3/MnO	13.25[a]	14.75[a]	9.85[a]	2.62[b]	28.07[a]	11.06[b]	NS	**	75.1

† *, ** Significant at the 0.05 and 0.01 probability levels; NS not significantly different at the 0.05 probability level.

‡ Within a comparison group of size or color, means of the same elemental oxide followed by the same letter are not significantly different at the 0.05 probability level.

https://doi.org/10.1346/CCMN.1997.0450312 Published online by Cambridge University Press

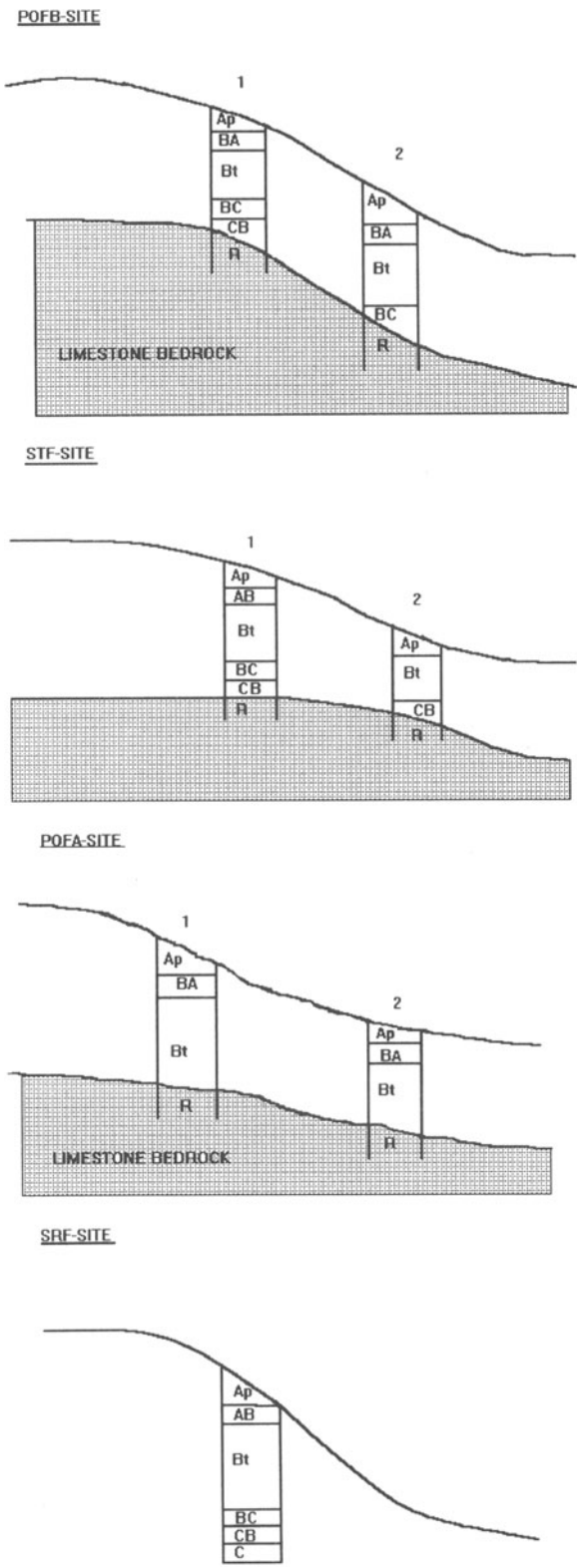

Figure 1. Soil topography and stratigraphy of the sites sampled.

oxides (MnCOP), amorphous (AM), Mn coprecipitated with Fe oxides (FeCOP) and crystalline Fe oxide (FeCRO) fractions. The elemental composition of selected concretionary material was determined by fusing a subsample (0.2 g, passed through a 10-μm sieve) with lithium metaborate ($LiBO_2$) (1:5 ratio), dissolving the fused sample in 4% HNO_3, and analyzing the solution for Si, Al, Fe, Mn, Ca, Mg, K, Na and Ti by atomic absorption spectrometry (AAS), and for P by colorimetry (Bartenfelder and Karathanasis 1988).

Mineralogical analyses were performed by XRD on whole concretionary materials (powder mounds) and separately on the <5-μm fraction (glass slide) before and after a citrate–bicarbonate–dithionite treatment. The <5-μm fractions were separated by centrifugation (Jackson 1956) following suspension in deionized water and dispersion in an ultrasonic water bath for about 2 min. The samples were spun at 300 rpm for 2.9 min using a DAMON-IEC DPR-6000 centrifuge (International Equipment Co., Needham Heights, Massachusetts). The XRD analysis was performed with a PW 1840 Philips diffractometer, equipped with Co*K*α radiation (40 kV, 30 mA) and a Si-diode detector (Karathanasis and Hajek 1982). All specimens were step-scanned from 2 to 80 °2θ at 0.5 °2θ increments with a counting time of 10 s per increment.

Micromorphological examinations were performed on selected soil thin sections prepared according to the procedures published by the Soil Survey Staff (1984), using a Leitz-Werner Ortholux petrographic microscope. Selected concretion specimens were also examined with a Hitachi S-800 field emission scanning electron microscope, equipped with a backscattered electron detector.

RESULTS AND DISCUSSION

Chemical Composition of Concretions

Mean values of elemental composition and analysis of variance for different size and color concretions from 5 Ap horizons and 4 Bt horizons of 6 pedons are given in Table 2. Among 10 elemental oxides, SiO_2 was the highest (41.11–51.86%). Iron oxide was second (26.43–33.76%), followed by Al_2O_3 (14.44–15.01%) and MnO (3.84–7.19%). All other elemental oxides averaged <2.3%. While the Al_2O_3 content was independent of concretion size, SiO_2 increased with decreasing size. The opposite was true for Fe_2O_3 and MnO, which were highest in coarser-size concretions. This is probably an indication that Si and Al in the concretions are associated with trapped soil material composed primarily of aluminosilicate minerals (more 2:1 minerals in the fine- than in the coarse-size concretions). Also, larger-size concretions appeared to be Fe-enriched

https://doi.org/10.1346/CCMN.1997.0450312 Published online by Cambridge University Press

Table 3. Elemental composition of concretions from selected horizons of 2 studied pedons.

Pedon	Horizon	Color	Size (mm)	SiO_2	Al_2O_3	Fe_2O_3	MnO	CaO	MgO	K_2O	Na_2O	TiO_2	P_2O_5	Total	Fe/Mn
								%							
POFB1	Ap	Black	>2	38.69	17.72	25.99	14.28	0.88	0.57	1.45	0.57	0.94	0.31	101.40	1.8
			2–1	46.03	18.28	22.96	10.73	0.57	0.43	1.07	0.66	0.84	0.31	101.88	2.1
			1–0.5	53.37	16.12	24.58	5.53	0.66	0.37	0.83	0.50	0.69	0.28	102.93	4.4
		Brown	>2	34.15	14.56	48.97	0.89	0.44	0.47	1.11	0.46	0.91	0.76	102.17	55.0
			2–1	39.84	15.20	40.26	0.69	0.46	0.47	1.16	0.35	0.85	0.53	99.81	58.3
			1–0.5	44.69	15.90	36.18	1.65	0.80	0.51	1.15	0.29	0.99	0.43	102.59	21.9
STF2	Bt1	Black	>2	43.00	16.66	26.06	11.09	1.70	0.49	0.96	0.31	0.80	0.77	101.84	2.4
			2–1	47.00	17.42	22.90	9.34	2.46	0.54	1.07	0.37	0.78	0.77	102.65	2.5
			1–0.5	50.96	17.60	19.00	7.47	2.73	0.45	1.02	0.84	0.76	0.83	101.66	2.5
		Brown	>2	40.28	12.80	35.37	2.90	5.75	0.57	0.84	0.42	0.85	0.96	100.74	12.2
			2–1	45.33	14.22	35.46	2.06	3.07	0.52	0.91	0.48	0.61	0.88	103.54	17.2
			1–0.5	49.71	16.22	20.03	5.22	7.02	0.70	1.05	0.28	0.80	1.03	102.06	3.8

(high Fe_2O_3/MnO ratio) compared to the fine-size concretions, which were Mn-enriched.

Elemental composition differences were also evident in different color concretions separated from Ap and Bt1 horizons of the POFB1 and STF2 sites, especially with respect to Fe_2O_3 and MnO content (Table 3). Although all concretions contained more Fe_2O_3 than MnO, brown concretions were much higher in Fe_2O_3, while black concretions had increased amounts of MnO. These differences were more prominent in coarse-size concretions. The Fe/Mn ratios in black concretions were relatively independent of size, but increased with increasing concretion size in brown concretions (Table 3).

The effect of concretion size on Fe_2O_3, MnO and SiO_2 composition of black and brown concretions selected from 2 sites is evident in Figure 2. For both color concretions, SiO_2 increased with decreasing size, while Fe_2O_3 remained unchanged or decreased with decreasing size, especially in brown concretions. In contrast, MnO decreases with decreasing size were evident only in the black concretions. These trends indicate that the formation, development and accumulation of Fe-Mn concretions is a dynamic and progressive translocation and transformation process of Fe and Mn in the soil profile.

Results of the sequential fractionation of Mn and Fe into exchangeable (EXCH), organic (OM), crystalline oxide (CRO), amorphous (AM), coprecipitated (COP) and total secondary (Total-S) forms among different concretion sizes are reported in Tables 4 and 5. Generally, the crystalline Mn-oxides appeared to dominate the Mn fraction in all size of concretions. However, considerable variability in their concentration existed among different pedons and horizons. With the exception of the SRF site, concretions in Bt horizons contained higher amounts of crystalline Mn than Ap horizons, with the highest amounts from the POFB2 site. There was no consistent trend for crystalline Mn distribution among different concretion sizes, although

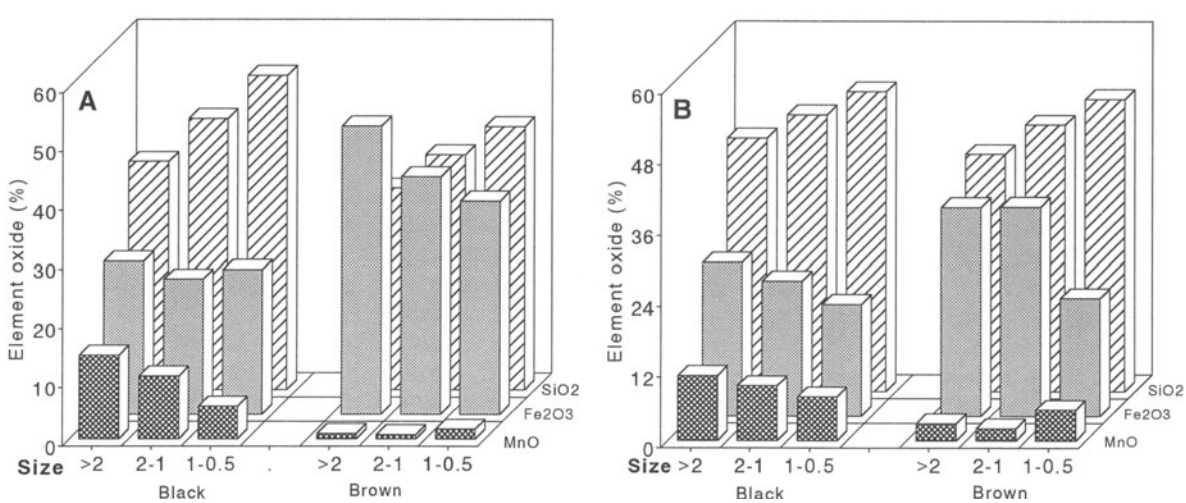

Figure 2. Comparison of MnO, Fe_2O_3 and SiO_2 contents in different size and color concretions. A) Concretions from pedon POFB1, Ap horizon; and B) concretions from pedon STF2, Bt1 horizon.

https://doi.org/10.1346/CCMN.1997.0450312 Published online by Cambridge University Press

Table 4. Distribution of various forms of secondary Mn among different-size concretions in selected soil horizons†.

Pedon	Horizon	>2 mm Concretions					2–1 mm Concretions					1–0.5 mm Concretions				
		EXCH	OM	CRO	AM	FeCOP	EXCH	OM	CRO	AM	FeCOP	EXCH	OM	CRO	AM	FeCOP
		Mn (mg/kg)														
POFA1	Ap	24	17	11,180	1620	990	30	11	4820	2150	970	25	22	3680	1785	965
	Bt1	33	27	18,900	1795	1255	24	15	6620	2005	1175	58	11	4920	3150	1125
POFA2	Ap	6	13	12,640	2270	1090	35	13	5140	1745	1010	58	17	4240	2155	1040
	Bt1	17	19	13,000	2005	1315	38	11	6200	2410	1260	23	9	5360	2160	1135
POFB1	Ap	6	19	7680	1230	1130	13	12	6860	1590	810	10	15	8160	2045	1335
	Bt2	16	67	19,400	3690	1850	61	60	18,260	1650	1730	44	23	15,820	1990	1925
POFB2	Ap	31	11	7480	940	1025	44	15	12,060	2650	1325	65	42	9240	2450	1065
	Bt2	152	71	24,080	2105	1840	194	79	17,660	1660	1585	188	45	19,980	8300	2335
STF1	Ap	58	73	13,440	4780	2485	70	31	12,700	6800	2630	93	67	8640	3295	1880
	Bt2	12	20	14,920	2555	2195	18	15	14,860	6200	2740	19	16	13,240	3545	2420
STF2	Ap	52	39	13,480	3290	2560	156	111	14,300	5040	2275	282	348	10,720	2735	1875
	Bt1	26	20	18,120	2785	1900	23	18	19,200	5530	2465	76	11	15,840	9450	2165
SRF	Ap	26	8	3200	3100	780	29	22	6780	3100	680	56	79	3360	3585	1110
	Bt3	44	5	2000	275	235	34	3	1780	250	360	65	5	3300	825	370

† Key: EXCH = exchangable Mn; OM = Mn associated with organic matter; CRO = crystalline Mn oxides; AM = amorphous Mn; and FeCOP = Mn coprecipitated with Fe oxides.

most of the high values were associated with coarser-size concretions.

The crystalline Fe-oxides were also the dominant Fe form in all sizes of concretions (Table 5). Exchangeable, organic and Mn-oxide coprecipitated Fe forms constituted only a very small proportion of the total secondary Fe. No consistent trends occurred with different sizes. Amorphous Fe generally increased with decreasing concretion size, but there was significant site variability. Concretions in STF1 and STF2 sites appeared to have higher amorphous Fe and lower crystalline Fe than other sites. This is probably due to lower clay content and greater water throughflow in their Bt horizons.

Mean and standard deviation values for secondary Mn and Fe distribution and analysis of variance among different-size concretions are shown in Table 6. In spite of the large variability, total secondary Mn usually increased with concretion size, and amorphous Mn tended to accumulate in smaller-size concretions. Conversely, the crystalline Mn oxides were more prominent in larger-size concretions (Table 6 and Figure 3a). Similar trends were found for the distribution of secondary Fe among different-size concretions (Table 6 and Figure 3b).

These relationships suggest that Mn and Fe precipitation in concretionary material occurs usually at a very slow rate from saturated but not supersaturated soil solutions. Under these conditions, crystalline oxides dominate over amorphous forms because the latter precipitate at a faster rate from supersaturated solutions. The fact that most crystalline oxides are concentrated in larger-size concretions is probably due to the higher frequency of oxidation–reduction cycles

Table 5. Distribution of various forms of secondary Fe among different-size concretions in selected soil horizons†.

Pedon	Horizon	>2 mm Concretions					2–1 mm Concretions					1–0.5 mm Concretions				
		EXCH	OM	MnCOP	AM	CRO	EXCH	OM	MnCOP	AM	CRO	EXCH	OM	MnCOP	AM	CRO
		Fe (mg/kg)														
POFA1	Ap	16.3	169	782	17,250	175,500	7.9	150	980	21,650	147,000	5.7	113	520	20,150	190,500
	Bt	16.2	152	476	12,900	148,500	2.8	201	1002	17,300	157,500	7.5	119	1058	25,550	132,000
POFA2	Ap	6.1	127	682	19,150	162,000	4.4	84	1056	16,000	143,500	5.5	114	750	20,750	113,500
	Bt1	5.0	172	558	18,650	176,500	4.0	142	934	19,600	146,500	2.0	102	746	19,600	93,500
POFB1	Ap	13.5	368	802	14,800	162,000	6.7	126	944	19,850	147,500	5.5	125	792	16,200	130,500
	Bt2	2.2	98	620	12,350	116,000	2.0	73	682	14,250	126,500	2.2	104	790	15,750	130,000
POFB2	Ap	2.9	149	786	14,150	191,500	10.5	119	800	18,050	147,500	15.0	119	770	18,200	101,000
	Bt2	1.0	157	286	12,700	131,000	3.4	141	594	15,400	150,500	1.4	61	546	47,550	89,500
STF1	Ap	7.1	102	738	32,500	142,500	2.1	99	760	48,550	98,000	1.7	65	738	25,400	65,000
	Bt2	2.9	98	640	24,650	123,500	5.5	57	684	37,600	74,000	1.8	61	612	21,650	50,000
STF2	Ap	3.0	126	78	21,600	106,500	4.8	49	702	34,800	86,000	2.8	36	792	18,000	60,500
	Bt1	3.7	82	440	24,550	142,000	4.1	70	608	41,000	68,000	3.8	154	590	50,400	75,550
SRF	Ap	9.2	161	480	27,150	139,000	10.9	82	920	29,650	99,500	11.3	55	480	27,900	101,000
	Bt3	3.5	225	464	34,450	159,500	3.1	136	488	24,100	136,000	4.2	141	764	32,800	139,000

† Key: EXCH = exchangable Fe; OM = Fe associated with organic matter; MnCOP = Fe coprecipitated with Mn oxides; AM = amorphous Fe oxides; and CRO = crystalline Fe oxides.

Table 6. Mean, standard deviation and analysis of variance (n = 14) for secondary Mn and Fe forms distributed among different-size concretions as determined by the sequential extraction procedure.

Fe–Mn forms	Concentrations (mg kg^{-1})			Analysis of variance	
	Coarse (>2 mm)	Medium (2–1 mm)	Fine (1–0.5 mm)	Size	CV (%)
EXCH-Mn†	35.9 ± 37.0[a]¶	54.9 ± 53.7[a]	75.9 ± 73.7[a]	NS§	105.7
OM-Mn	29.1 ± 23.8[a]	29.7 ± 31.4[a]	50.7 ± 88.5[a]	NS	148.4
CRO-Mn	14,251 ± 8345[a]	10,517 ± 5721[a]	9036 ± 5412[a]	NS	51.0
AM-Mn	2317 ± 1175[a]	3058 ± 2003[a]	3391 ± 2453[a]	NS	67.0
FeCOP-Mn	1475 ± 678[a]	1501 ± 763[a]	1482 ± 612[a]	NS	47.4
Total-S Mn	18,019 ± 9591[a]	15,159 ± 7714[b]	14,034 ± 7901[b]	*	48.8
EXCH-Fe‡	6.6 ± 5.2[a]	5.2 ± 3.0[a]	5.1 ± 4.0[a]	NS	69.5
OM-Fe	156.1 ± 71.8[a]	109.2 ± 42.9[b]	97.8 ± 35.8[b]	*	44.1
MnCOP-Fe	559 ± 208[b]	797 ± 177[a]	711 ± 150[a]	**	25.4
AM-Fe	21,918 ± 7530[a]	25,557 ± 10,908[a]	25,707 ± 10,942[a]	NS	40.9
CRO-Fe	148,286 ± 24,442[a]	123,428 ± 31,435[b]	105,107 ± 37,645[b]	**	26.0
Total-S Fe	171,719 ± 23,473[a]	149,897 ± 22,877[b]	131,628 ± 36,856[b]	**	19.8

† Key: EXCH-Mn = exchangable Mn; OM-Mn = Mn associated with organic matter; CRO-Mn = crystallin Mn oxides; AM-Mn = amorphous Mn; FeCOP-Mn = Mn coprecipitated with Fe oxides; and Total-S Mn = total secondary Mn.

‡ Key: EXCH-Fe = exchangable Fe; OM-Fe = Fe associated iwth organic matter; MnCOP-Fe = Fe coprecipitated with Mn; AM-Fe = amorphous Fe; CRO-Fe = crystalline Fe oxides; and Total-S Fe = total secondary Fe.

§ *, ** Significant at the 0.05 and 0.01 probability levels; NS not significant at the 0.05 probability level.

¶ Within a comparison group of size, means ± SD of the same forms of secondary Mn or Fe followed by the same letter are not significantly different at the 0.05 probability level.

and length of oxidation periods occurring above the restrictive horizons, where the larger-size concretions are common. These conditions induce multiple layers of Fe and Mn precipitation on existing smaller-size nodules, resulting in a size increase, which is accentuated by better porosity and aeration in these horizons.

Mineralogy of Concretions

X-ray diffraction analysis of whole concretionary materials did not show distinct peaks of Fe and Mn oxide minerals due to interference from very high quartz peak intensities. The XRD patterns of the <5-μm fractions provided better resolution, but only goethite was detectable. Representative XRD patterns of concretions with different size and color separated from the Ap horizon of pedon POFB1 are shown in Figure 4. Goethite was identified from reflections at 0.420, 0.269, 0.271, 0.171 and 0.145 nm, regardless of concretion size and color. Its presence is supported by the concretion fractionation data, which showed the crystalline Fe oxides to be the dominant Fe component (CBD extraction). The amorphous Fe amounted to about ⅕ to 1/10 of the crystalline Fe oxides. No crystalline Mn-oxide minerals were identified, even in concretions with the highest Mn concentration (>2 mm

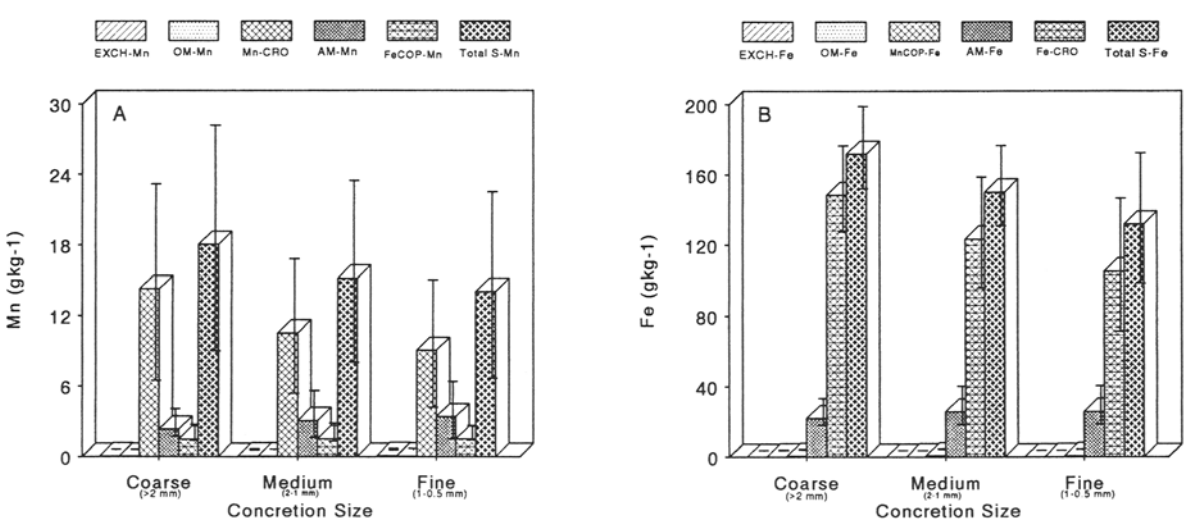

Figure 3. Comparison of various forms of secondary Mn A) and secondary Fe B) in different-size concretions.

https://doi.org/10.1346/CCMN.1997.0450312 Published online by Cambridge University Press

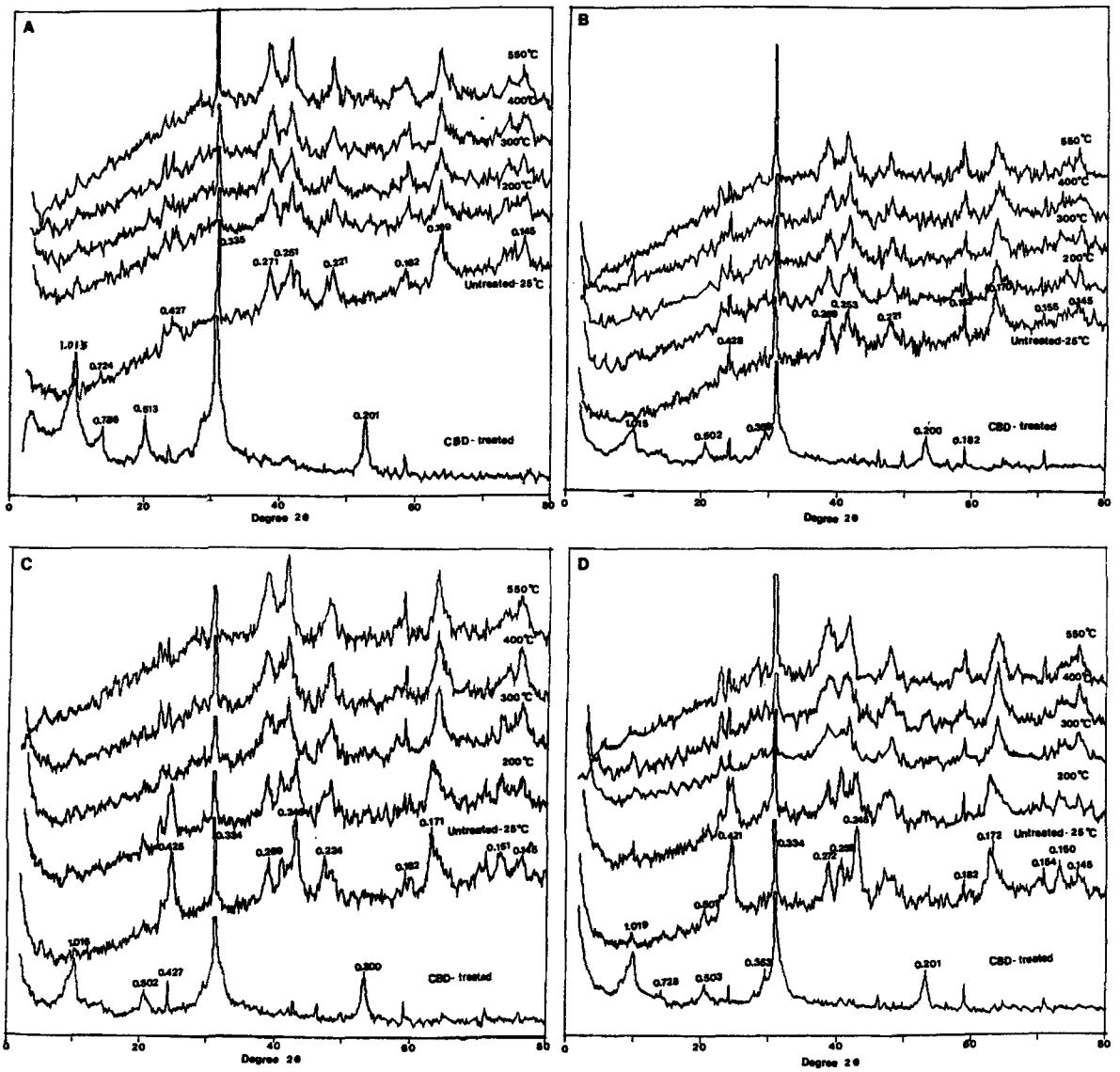

Figure 4. XRD patterns of different size and color concretions (<5-μm fractions) untreated and treated with CBD from pedon POFB1, Ap horizon. A) Coarse (>2 mm) black concretions; B) medium (2–1 mm) black concretions; C) coarse (>2 mm) brown concretions; and D) medium (2–1 mm) brown concretions.

black concretions with 14.28% MnO from pedon POFB1, Ap horizon, Table 3).

Other minerals present in the <5-μm concretionary fraction were mica (1.015, 0.502 nm), kaolinite (0.724, 0.359 nm) and quartz (0.334, 0.182 nm). The presence of goethite (0.420, 0.269, 0.271, 0.220, 0.171, 0.151, 0.145 nm) was confirmed by the reduction of the broad peaks in the 0.420 region following CBD treatment, which allowed a better resolution of the 0.425 reflection of quartz (Figure 4). Upon heating to 400 and 550 °C, the 0.420, 0.418 and 0.151 nm peaks decreased, while the 0.269, 0.251 and 0.145 nm peaks were enhanced (Figure 4), indicating transformation of goethite to hematite (Tokashiki et al. 1986).

Another noticeable difference in the XRD patterns is the increased sharpness/intensity of the goethite peaks from the brown concretions that had a higher total Fe oxide content than the black concretions (Figure 4 and Table 3). Goethite peak intensities also increased with crystalline Fe oxide content and increasing concretion size (Figure 4 and Table 6). Similar trends between goethite and Fe oxide content were observed for all pedons.

https://doi.org/10.1346/CCMN.1997.0450312 Published online by Cambridge University Press

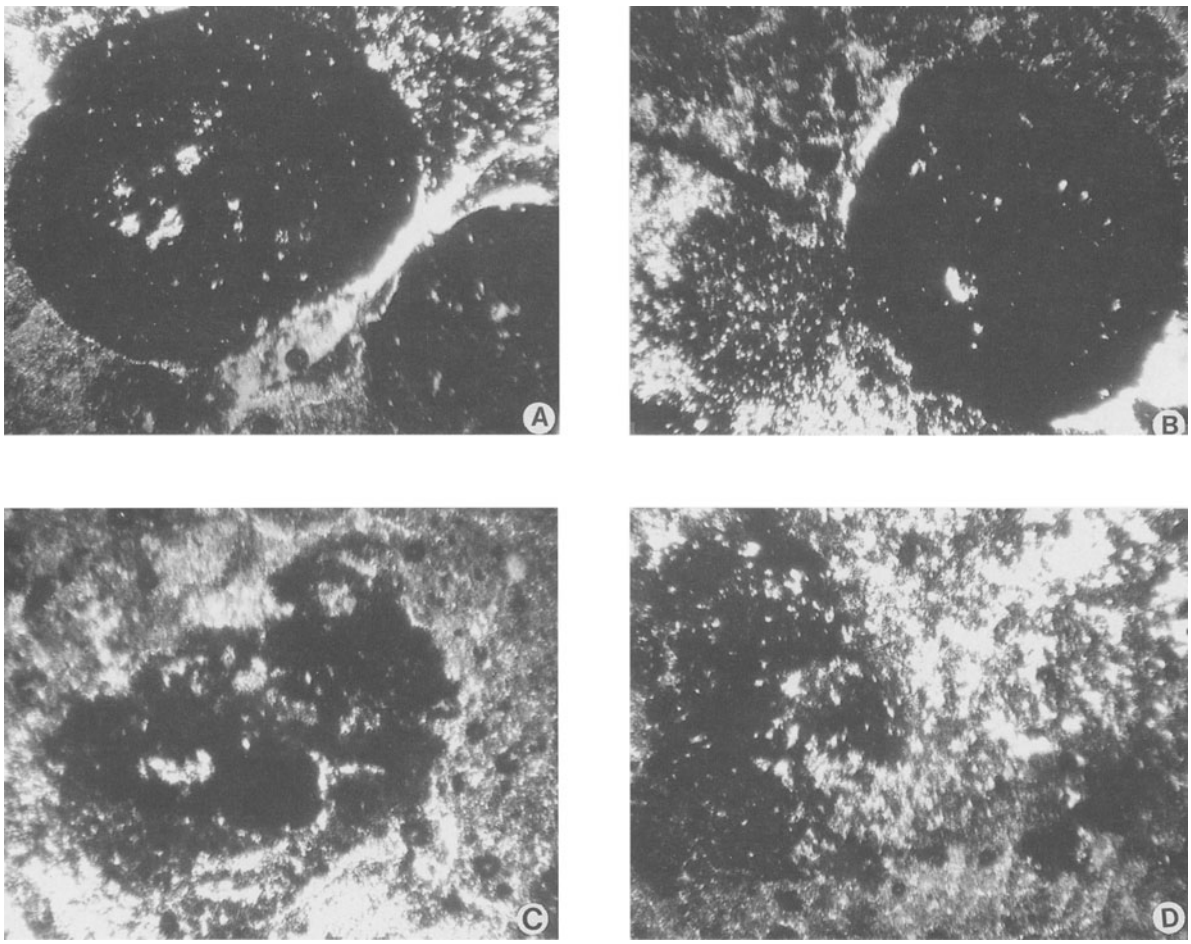

Figure 5. Representative micrographs of Fe-Mn concretions from soil thin sections in different horizons. A) Brown concretion from pedon POFB1, BA horizon (perching water zone); B) black concretions from the same horizon as graph A; C) black concretion from pedon STF1, Bt2 horizon (restrictive layer); and D) black ferromangan soft masses (stains), from pedon STF1, CB horizon (perched water table zone above the lithic limestone interface).

Micromorphology of Concretions

Micrographs of selected Fe-Mn concretions in soil thin sections from the BA horizon of pedon POFB1, and Bt2 and CB horizons of pedon STF1, are shown in Figure 5. Concretions from perched water zones showed a more dense differentiated fabric, sharp external boundaries and generally a spherical shape (Figures 5a and 5b). Constituents were usually arranged in diffuse zones or bands around a central point, often a quartz grain or a void. Concentric banding in concretions has been attributed to frequently alternating oxidation–reduction periods. For the soils studied, these conditions are prevalent within water perching horizons above restrictive clayey layers, which have lower clay contents and extensive macroporosity that favors concretion formation.

In contrast, concretions within clayey restrictive horizons (Figure 5c) showed a less-differentiated internal fabric, somewhat irregular in shape, and distinct to diffuse external boundaries. This is probably due to their dense soil matrix and limited pore space, which hinder the development of distinct bands and sharp external concretion boundaries.

The Fe and Mn concretions from perched water table-affected zones overlying limestone bedrock interfaces were lacking the hardness and organization found in upper solum horizons. Because of the longer duration and greater frequency of saturation, considerably higher amounts of Fe and Mn are dissolved in these zones and produce the observed gray chroma matrix with common distinct or prominent bright Fe (ferrans) and black Mn (mangans) soft masses. However, these soil zones are saturated or are moisture-enriched for too long to allow extensive hardening of Mn and Fe (concretion formation) to occur. Figure 5d illustrates an Fe-Mn soft mass with agglomeroplasmic fabric in the CB horizon of the STF1 pedon.

https://doi.org/10.1346/CCMN.1997.0450312 Published online by Cambridge University Press

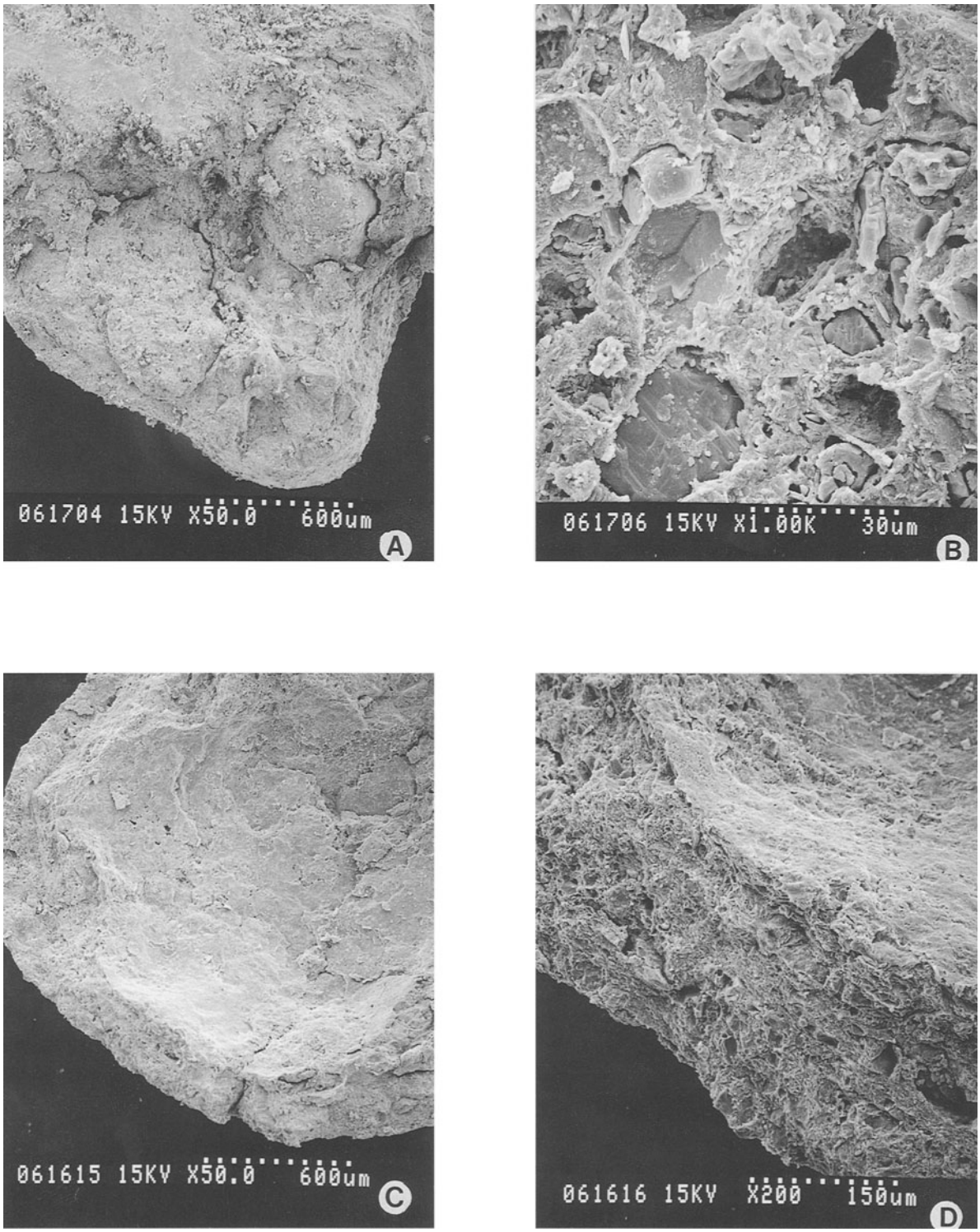

Figure 6. SEMs of Fe-Mn concretions from the Ap horizon, pedon POFB1. A) A cleaved coarse (>2 mm) brown concretion showing round dense clay cores; B) quartz and other mineral crystal grains inside a coarse brown concretion; C) a cleaved coarse black concretion showing concentric bands; and D) a magnified cross section of the concentric bands shown in Figure 5c.

https://doi.org/10.1346/CCMN.1997.0450312 Published online by Cambridge University Press

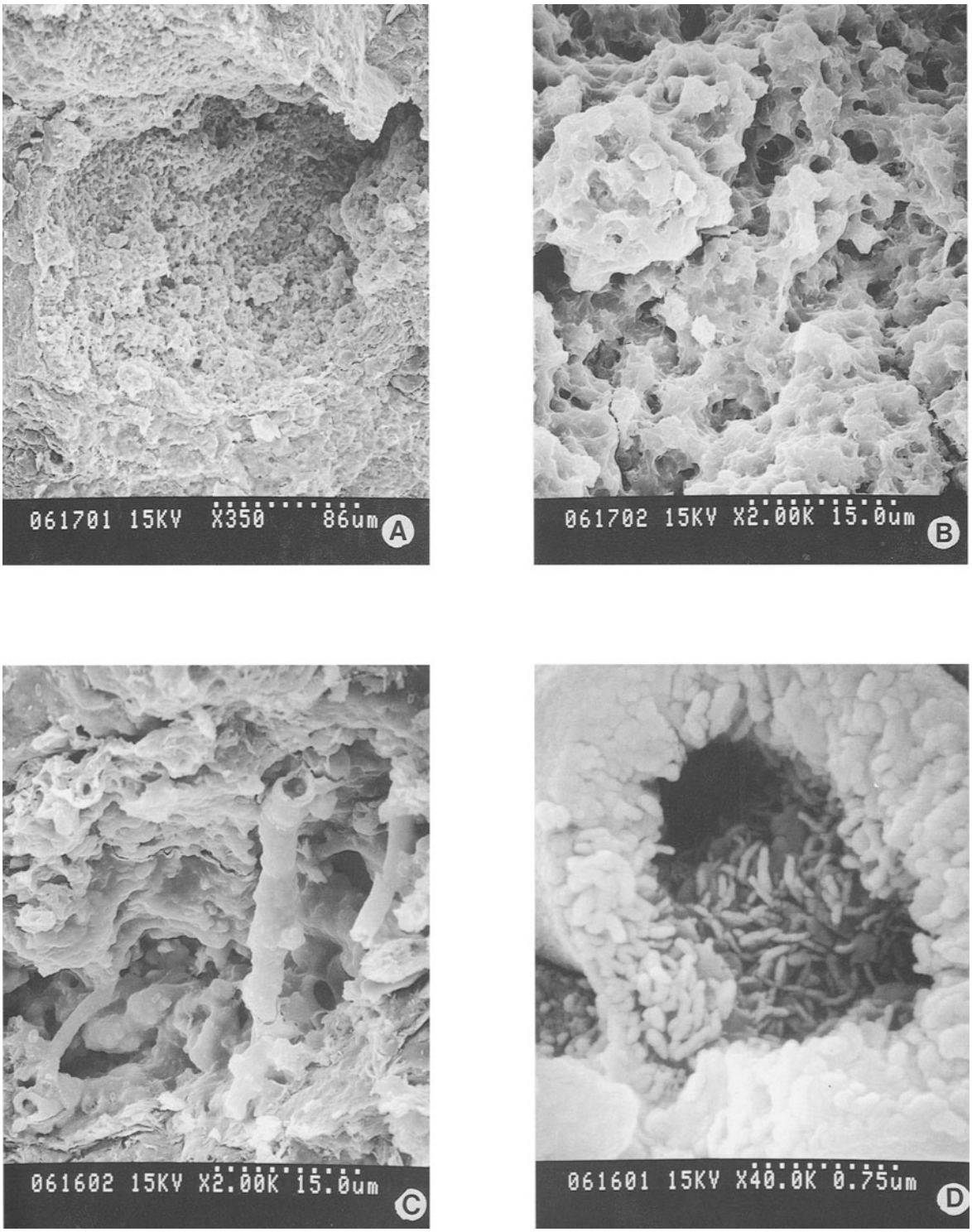

Figure 7. SEMs showing the macropore and micropore structure of Fe-Mn concretions from the Ap horizon of pedon POFB1. A) A cavity inside a concretion; B) a magnified section of the cavity shown in Figure 6a showing the cheese-like matrix and microporosity of the concretion; C) tubularly shaped Mn-enriched features coating the surface of a concretion cavity; D) clusters of accicularly shaped goethite crystals inside a concretion cavity.

https://doi.org/10.1346/CCMN.1997.0450312 Published online by Cambridge University Press

Micrographs of selected concretion specimens examined by SEM are illustrated in Figures 6 and 7.Many coarse (>2 mm) concretions, especially those brown in color, contained randomly distributed quartz grains and round dense clay cores cemented by Fe and Mn oxides (Figures 6a and 6b). Both features were embedded in the concretion matrix but exhibited distinct boundaries. Although each feature appeared to occupy cavities within the matrix, they probably formed the original nucleus around which additional concretionary material was attached. Figure 6c shows a micrograph of the interior of a cleaved coarse black concretion, spherical in shape, from which the denser core was separated during the specimen preparation process. The concentric bands or layers representing cyclic Fe-Mn precipitation periods are evident, especially in the cross section of Figure 6d.

Most concretions, in spite of their dense morphology, also appeared to have a sizeable macropore–micropore network. The macropore features observed, however, appeared to be nonconducting dead-end cavities. Considerable detail of such a cavity is shown in Figure 7a. The micropore structures (cheese-like) of the concretionary matrix is illustrated in a magnified sector of the cavity in Figure 7b. Other infilling features of cavities found in the interior of some concretions are shown in Figures 7c and 7d.

Figure 7c illustrates Mn-enriched tubes coating the surface of a macropore cavity. This pattern may indicate microbial involvement in the Mn-precipitation process. Other cavities, such as the one illustrated in Figure 7d, were half-filled with aggregate overgrowths of acicular goethite crystals. Similar infillings of Fe and Mn are bound to occur at a smaller-size scale within the micropore system and eventually produce the dense concretionary matrix structure. These infillings are probably the result of diffusion of dissolved plasmic Fe and Mn and subsequent precipitation within the pore volume of the concretionary matrix.

SUMMARY AND CONCLUSIONS

This study conducted in the Inner Bluegrass Region of Kentucky examined changes in the macro- and micromorphology, chemistry and mineralogy of Fe-Mn concretions as a function of size, color and soil depth. The chemical composition of the concretions varied with concretion size and color. All of the black concretions contained higher amounts of Mn, while brown concretions were higher in Fe. Total Mn and Fe increased, while SiO_2 decreased with concretion size. Similarly, crystalline Mn- and Fe-oxides fractionated with a sequential extraction procedure increased, but amorphous Mn and Fe decreased with increasing concretion size. With regards to concretion mineralogy, goethite was the only crystalline Fe oxide mineral identified by XRD analysis. Manganese oxide minerals could not be detected due to the diffuse nature of their XRD peaks and poor crystallinity. Examination of soil thin sections showed that accumulation patterns and characteristics of Fe-Mn concretions in Kentucky Alfisols are strongly influenced by perched water tables. Concretions of soil horizons overlying restrictive clayey layers exhibited differentiated fabrics, sharp external boundaries and generally spherical shapes. Concretions found within clayey restrictive layers or above lithic interfaces usually had less structural organization, softer matrices and diffuse external boundaries due to longer-term saturation conditions. Scanning electron microscopy examinations suggested that the concretionary matrix, in spite of its density, has numerous cavities and an extensive micropore system within which dissolved plasmic Fe and Mn can diffuse and precipitate.

REFERENCES

Bartenfelder DC, Karathanasis AD. 1988. A comparison between X-ray fluorescence and dissolution methods employing lithium metaborate fusion for elemental analysis of soil clays. Commun Soil Sci Plant Anal 19:471–492.

Barnhisel RI, Phillippe WR, Blevins RL. 1969. A simple X-ray fluorescence technique for the determination of iron and manganese in soils and concretions. Soil Sci Soc Am Proc 33:811–813.

Cescas MP, Tyner EH, Harmer III RS. 1970. Ferromanganiferous soil concretions: A scanning electron microscope study of their micropore structures. Soil Sci Soc Am Proc 34:641–644.

Drosdoff M, Nikiforoff CC. 1940. Iron-manganese concretions in Dayton soils. Soil Sci 49:333–345.

Gallaher RN, Perkins HF, Radcliffe D. 1973a. Soil concretions: I. X-ray spectrograph and electron microprobe analysis. Soil Sci Soc Am Proc 37:465–469.

Gallaher RN, Perkins HF, Tan KH, Radcliffe D. 1973b. Soil concretions: II. Mineralogical analysis. Soil Sci Soc Am Proc 37:469–472.

Jackson ML. 1956. Soil chemical analysis—Advanced course. Madison, WI: ML Jackson. 893 p.

Karathanasis AD, Hajek BF. 1982. Revised methods for rapid quantitative determination of minerals in soil clays. Soil Sci Soc Am J 46:419–425.

McDaniel PA, Bathke GR, Buol SW, Cassel DK, Falen AL. 1992. Secondary manganese/iron ratios as pedochemical indicators of field-scale throughflow water movement. Soil Sci Soc Am J 56:1211–1217.

McDaniel PA, Buol SW. 1991. Manganese distribution in acid soils of the North Carolina Piedmont. Soil Sci Soc Am J 55:152–158.

Murthy RS, Mathur BS. 1964. Special formation in some alluvial soil profiles of the Ganga river plain of Central Uttar Pradesh—Their origin, development and significance [abstract]. Soils Fert Abstr 31:148.

Phillippe WR, Blevins RL, Barnhisel RI, Bailey HH. 1972. Distribution of concretions from selected soils of the inner bluegrass region of Kentucky. Soil Sci Soc Am Proc 36: 171–173.

Radden JA, Porter HC. 1962. Preliminary note on some soil concretions in the Virginia Piedmont. Mineral Ind J 9:1–4.

Rhoton FE, Bigham JM, Schulze DG. 1993. Properties of iron-manganese nodules from a sequence of eroded fragipan soils. Soil Sci Soc Am J 57:1386–1392.
Rhoton FE, Meyer LD, McChesney DS. 1991. Depth of erosion assessment using Fe-Mn nodule concentrations in surface horizons. Soil Sci 152:389–394.
Ross SJ. Jr, Franzmeier DP, Roth CB. 1976. Mineralogy and chemistry of manganese oxides in some Indiana soils. Soil Sci Soc Am J 40:137–143.
Schwertmann U, Fanning DS. 1976. Iron-manganese concretions in hydrosequences of soils in loess in Bavaria. Soil Sci Soc Am J 40:731–738.
Shuman LM. 1985. Fractionation method for soil microelements. Soil Sci 140:11–22.
Soil Survey Staff. 1984. Procedures for collecting soil samples and method of analysis for soil survey. Soil Survey Invest Rep 1. Washington, DC: US GPO. 248 p.
Tokashiki Y, Dixon JB, Golden DC. 1986. Manganese oxide analysis in soils by combined X-ray diffraction and selective dissolution methods. Soil Sci Soc Am J 50:1079–1084.
Uzochukwu GA, Dixon JB. 1986. Manganese oxide minerals in nodules of two soils of Texas and Alabama. Soil Sci Soc Am J 50:1358–1363.
Winters Eric. 1938. Ferromanganiferous concretions from some podzolic soils. Soil Sci 46:33–40.

(Received 22 January 1996; accepted 29 July 1996; Ms. 2731)